



HAL
open science

Improved ZT in ball-milled and spark plasma sintered Cu₁₅As₃₀Te₅₅ glass ceramics

Cédric Morin, Judith Monnier, Jean-baptiste Vaney, Gaëlle Delaizir, Andrea Piarristeguy, Christophe Candolfi, Annie Pradel, Bertrand Lenoir, Eric Alleno

► **To cite this version:**

Cédric Morin, Judith Monnier, Jean-baptiste Vaney, Gaëlle Delaizir, Andrea Piarristeguy, et al.. Improved ZT in ball-milled and spark plasma sintered Cu₁₅As₃₀Te₅₅ glass ceramics. *Journal of the American Ceramic Society*, 2018, 10.1111/jace.16137 . hal-02049201

HAL Id: hal-02049201

<https://hal.science/hal-02049201>

Submitted on 1 Mar 2019

HAL is a multi-disciplinary open access archive for the deposit and dissemination of scientific research documents, whether they are published or not. The documents may come from teaching and research institutions in France or abroad, or from public or private research centers.

L'archive ouverte pluridisciplinaire **HAL**, est destinée au dépôt et à la diffusion de documents scientifiques de niveau recherche, publiés ou non, émanant des établissements d'enseignement et de recherche français ou étrangers, des laboratoires publics ou privés.



**Improved ZT in ball-milled and spark plasma sintered
Cu₁₅As₃₀Te₅₅ glass-ceramics**

Journal:	<i>Journal of the American Ceramic Society</i>
Manuscript ID	JACERS-42371.R1
Manuscript Type:	Article
Date Submitted by the Author:	n/a
Complete List of Authors:	Monnier, Judith; Université Paris Est Créteil, ICMPE Morin, Cédric; Université Paris-Est Créteil, ICMPE Vaney, J.; Institut Jean Lamour Delaizir, Gaëlle; Institut de Recherche sur les Céramiques Piarristeguy, Andrea; Institut Charles Gerhardt de Montpellier Candolfi, Christophe; Institut Jean Lamour Pradel, Annie; Institut Charles Gerhardt de Montpellier Lenoir, Bertrand; Institut Jean Lamour Alleno, Eric; Université Paris Est Créteil, ICMPE
Keywords:	thermoelectric properties, chalcogenides, glass-ceramics
Author-supplied Keyword: If there is one additional keyword you would like to include that was not on the list, please add it below::	ball-milling

SCHOLARONE™
Manuscripts

Improved ZT in ball-milled and spark plasma sintered $\text{Cu}_{15}\text{As}_{30}\text{Te}_{55}$ glass-ceramics

C. Morin¹, J. Monnier¹, J.B. Vaney², G. Delaizir³, A. Piarristeguy⁴, C. Candolfi², A. Pradel⁴,

B. Lenoir² and E. Alleno^{1*}

¹*Université Paris-Est, Institut de Chimie et des Matériaux Paris-Est, UMR 7182 CNRS – UPEC, 2 rue*

H. Dunant, 94320 THIAIS, France

²*Institut Jean Lamour (IJL), UMR 7198 CNRS-Université de Lorraine, France*

³*Institut de Recherche sur les Céramiques (IRCER), UMR CNRS 7315, Centre Européen de la*

Céramique, Limoges, France

⁴*Institut Charles Gerhardt (ICG), UMR 5253 CNRS-Université de Montpellier, France*

Abstract

The influence of ball-milling followed by Spark Plasma Sintering (SPS) on the thermoelectric properties of the $\text{Cu}_{15}\text{As}_{30}\text{Te}_{55}$ glass composition has been investigated by means of X-ray diffraction, scanning electron microscopy and differential scanning calorimetry. The microstructure, composition and thermal stability of the ball-milled samples before and after SPS have been correlated with the electrical and thermal transport properties. Upon ball-milling, a glass-to-glass transformation is evidenced for short ball-milling times, followed by crystallization of the metastable $\beta\text{-As}_2\text{Te}_3$ phase within the glassy matrix. This glass-to-glass transformation favors the occurrence of the $\beta\text{-As}_2\text{Te}_3$ phase during the SPS process. A maximum figure of merit ZT of 0.29 at 400K is obtained in the sample exhibiting the largest $\beta\text{-As}_2\text{Te}_3$ crystalline fraction. This ZT value is twice as high as the value obtained for the glass-ceramic sintered from non-ball-milled powder.

Keywords: Thermoelectric materials, ball milling, chalcogenide glass-ceramics

1. Introduction

Thermoelectric devices can be used as refrigerators (Peltier effect) or as electric power generators (Seebeck effect) since they can either pump heat or convert it into electricity. Their conversion efficiency is related to the dimensionless figure of merit ZT of the constituting materials defined by $ZT = \alpha^2 T / \rho \lambda$ where α is the Seebeck coefficient or thermopower, ρ is the electrical resistivity, λ is the total thermal conductivity and T is the absolute temperature. This technology is currently considered for supplying low electrical power ($\sim 1 \mu\text{W}$) to sensors by harvesting heat from ambient air or for medium power generation ($\sim 100 \text{ W}$) by recycling the heat wasted for instance by the exhaust pipe of cars.

Owing to their inherent disordered nature, chalcogenide glasses harbor extremely low thermal conductivity ($\sim 0.2 \text{ W}\cdot\text{m}^{-1}\cdot\text{K}^{-1}$) which is, however, at the expense of good electrical property with very large electrical resistivity (typically $\sim 100 \Omega\cdot\text{m}$)^{1, 2}. Upon metal substitution, their electrical resistivity can be nevertheless reduced by several orders of magnitude ($\sim 1 \text{ m}\Omega\cdot\text{m}$). Since they display large Seebeck coefficients ($\sim 500 \mu\text{V K}^{-1}$)², they have been considered as potential thermoelectric materials for room temperature applications³⁻⁵. Modifying the composition of these glasses is nonetheless insufficient to ensure a large thermoelectric figure of merit competing with state-of-the-art materials such as crystalline Bi_2Te_3 , which displays $ZT = 1$ at 300K. This ascertainment led to the partial crystallization approach of the glassy phase, which in the Cu-As-Te system, yields glass – ceramics materials with a complex multiscale nano/microstructure displaying ZT values of up to 0.08 at 300K⁶. In such glass-ceramic materials prepared from the peculiar $\text{Cu}_{15}\text{As}_{30}\text{Te}_{55}$ glass composition, the promoted crystalline phase is the metastable $\beta\text{-As}_2\text{Te}_3$ phase which by itself, is an interesting thermoelectric material with maximum ZT of 0.3 at 300 K upon proper optimization⁷. However, our recent study on glass-crystal composites ($\text{Si}_{10}\text{As}_{15}\text{Te}_{75}$ (glass) and $\text{Bi}_{0.4}\text{Sb}_{1.6}\text{Te}_3$ (crystal))⁸, combining experiments and generalized effective medium

theory-based (GEMT) calculations of the thermoelectric properties⁹⁻¹³, ruled out the possibility for a composite to reach ZT values larger than any of its component. Nonetheless, the GEMT was in most cases verified in composites which were constituted by mixtures of micrometric phases and very seldom checked on mixtures of nanometric phases, for which interface effects cannot be neglected. Hence, a reduction to the nanoscale of the typical size of the phases in the Cu-As-Te – As₂Te₃ glass - ceramic material was undertaken in the present work in order to determine whether improved thermoelectric properties could be achieved. To this end, high energy ball-milling was carried out in order to decrease the size of the Cu₁₅As₃₀Te₅₅ glass particles, prior to the crystallization process obtained by Spark Plasma Sintering⁶. Our results show that the influence of the particle size reduction to the nanoscale on the thermoelectric properties can be still well understood within the EMTs. The maximum ZT value of the composite is nonetheless strongly enhanced due to a fraction of crystalline phase larger than that achieved in non-ball-milled samples.

2. Experimental procedures

2.1. Synthesis and ball milling of the Cu₁₅As₃₀Te₅₅ glass powders

The Cu₁₅As₃₀Te₅₅ glass composition was synthesized by the conventional melt-quenching technique. A series of stoichiometric composition using highly-pure As (Ingots, Goodfellow, 99.99%), Te (Pellets, 5N+, 99.999%) and Cu (Beads, Sigma-Aldrich, 99.999%) were melted at 1123 K in a silica tube sealed under secondary vacuum and water-quenched⁶. The resulting ingots (~2 g) were hand-ground in an agate mortar, then analyzed by powder X-ray diffraction (PXRD) on a Bruker D8 diffractometer (Cu K α radiation) equipped with a Vantec 1D detector and by differential scanning calorimetry (DSC, TA Q100) in order to check that they are identical before being combined in a single batch. This Cu₁₅As₃₀Te₅₅ glass batch was dispatched in several 4g samples and milled using a Fritsch P7 premium planetary

1
2
3 machine equipped with 80 mL stainless steel jars at a speed of 500 rpm (round per minute).

4
5 The ball-to-powder ratio (BPR) was 15/1, with stainless balls of 2 mm in diameter. A first
6
7 batch was incrementally ball-milled up to $t_{BM} = 360$ min by sampling 20 mg of powder from
8
9 the vial inside a Ar-filled glove box at $t = 2, 8, 20, 45, 90, 180$ and 360 min. This sampled
10
11 powder was used to record a PXRD pattern (with a sample holder protecting the powder from
12
13 the air), to carry out a scanning electron microscopy (SEM) investigation and for DSC
14
15 measurements with a $10\text{ }^{\circ}\text{C min}^{-1}$ heating rate. Three other batches were ball-milled without
16
17 interruption during $t_{BM} = 20, 45, 130$ min. They were also characterized by PXRD (with a low
18
19 noise single-crystalline Si sample holder) and by DSC. These two different ball milling
20
21 conditions (with and without interruptions) may slightly influence the temperature inside the
22
23 vial and consequently the crystallization kinetics, even if large majority of the energy is
24
25 provided by the chocks.
26
27
28
29

30 31 2.2. Spark Plasma Sintering (SPS)

32
33 The elaboration conditions of the different $\text{Cu}_{15}\text{As}_{30}\text{Te}_{55}$ pellets are summarized in
34
35 Table 1 and are described below. The $\text{Cu}_{15}\text{As}_{30}\text{Te}_{55}$ powders milled for different durations
36
37 ($t_{BM} = 0, 20, 45, 130$ and 360 min) were sintered by SPS using a Dr. Sinter 505 Syntex
38
39 apparatus to obtain glass-ceramic materials. It is noteworthy that for this specific SPS
40
41 equipment, there is no way to bridle the intensity delivered by the generator (up to 1500 A).
42
43 For each ball-milling time t_{BM} , 3 samples were elaborated for reproducibility concerns. 0.7 g
44
45 of powder was introduced in an 8 mm diameter graphite die. The sintered temperature was
46
47 checked by a thermocouple located in the wall of the die. In order to follow the evolution of
48
49 the crystallization, 3 dwell times were applied (0, 10 and 20 min) at 423 K. An initial pressure
50
51 of 50 MPa was implemented for $t_{BM} = 0, 130$ and 360 min. Given the larger number of
52
53 crystallized phases obtained as compared to a previous study ⁶, the following ball-milled
54
55
56
57
58
59
60

1
2
3 samples ($t_{\text{BM}} = 20$ and 45 min) and another reference sample ($t_{\text{BM}} = 0$ min) were sintered
4
5 under a higher pressure of 80 MPa. However, as it will be discussed below (see $t_{\text{BM}} = 0$ min in
6
7 Table 1), the applied pressure is not a significant parameter in this study compared to other
8
9 parameters. In the case of $t_{\text{BM}} = 0$ min, an extra sample was synthesized with a 30 min dwell
10
11 time under 80 MPa. In the following, the powder obtained from hand-ground $\text{Cu}_{15}\text{As}_{30}\text{Te}_{55}$
12
13 glass ($t_{\text{BM}} = 0$ min) will be considered as a reference in this work. Figure 1 shows a
14
15 representative SPS cycle used to elaborate glass-ceramics. The temperature rises at a heating
16
17 rate of 90 K min^{-1} up to $T = 390 \text{ K}$. At this temperature, the heating rate is decreased to 45 K
18
19 min^{-1} to reach the dwell temperature of 423 K . As shown in Fig. 1 (a), an overshoot (T_{max}) can
20
21 be seen before the set-temperature plateau. At the end of the dwell time, the sample undergoes
22
23 a natural cooling. The density d of the samples was measured using the Archimedes's method
24
25 and is presented in Table 1. An average density of $d = 6.28 \pm 0.05 \text{ g.cm}^{-3}$ over all the samples
26
27 can be deduced. The standard deviation of 0.05 g.cm^{-3} is equal to the uncertainty of the
28
29 measurement. Thus, there is no significant variation in the density with the duration of the
30
31 initial ball-milling or the SPS parameters.
32
33
34
35
36

37 2.3. Transport properties of SPS glass-ceramics

38
39 Electrical resistivity measurements were directly performed on the SPS pellets with
40
41 parallel faces using the van der Pauw technique¹⁴. The thermal diffusivity a was measured by
42
43 the laser flash technique (Netzsch LFA 427) between 300 and 380 K. A piece of the sample
44
45 was used to measure the heat capacity C_p from room temperature up to 400 K with a Netzsch
46
47 Pegasus DSC apparatus, in order to calculate the thermal conductivity $\lambda = a \times C_p \times d$ where
48
49 d is the experimental density.
50
51

52
53 The Seebeck coefficient was measured between room temperature and 400 K on a
54
55 parallelepiped-shaped (about $1 \times 1 \times 8 \text{ mm}^3$) sample cut with a diamond wire saw. These
56
57

1
2
3 measurements were carried out using a homemade apparatus based on the differential method
4
5 ¹⁴. Measurement uncertainties are estimated to be 3% for Seebeck coefficient, 5% for
6
7 electrical resistivity, 10% for thermal conductivity and 15% for ZT ¹⁵.
8

9
10 Finally, the samples used for the Seebeck coefficient measurements were hand-ground
11 and PXRD was performed in the 2θ range 20-60° in order to determine the nature of the
12 crystalline phases stabilized in the glass-ceramics. The amount of residual glass was estimated
13 by integrating the area under the main XRD peak around $2\theta = 29.58^\circ$, normalized to the high
14 angle background. Moreover, the amount of α -As₂Te₃, β -As₂Te₃, AsTe and Cu_{1.4}Te
15 crystalline phases in the SPS samples was evaluated from Rietveld refinements.
16
17
18
19
20
21
22
23

24 3. Results and discussion

25 3.1 Structural, microstructural and thermal characterizations of ball milled Cu₁₅As₃₀Te₅₅ glass

26
27 Figure 2 shows SEM micrographs corresponding to the glass particle size reduction
28 after ball-milling. After 2 minutes, the particle size is reduced from hundreds of microns
29 (Fig.2a) to about 10-20 μm (Fig.2b). After 20 and 360 minutes (Fig.2c and 2d), the SEM
30 picture shows very small particles typically less than 1 μm . However, some larger particles,
31 up to 5 μm , are still present. Larger magnification (Fig. 2e-g) indicates that these particles are
32 aggregates of grains smaller than 100 nm.
33
34
35
36
37
38
39
40
41
42
43

44 Ball-milling effects in the Cu₁₅As₃₀Te₅₅ glass samples were also followed by PXRD.
45 In Fig.3, a + 0.6° shift in 2-theta for the main **broad peak** is noticeable around 29°, between
46 the non-ball-milled glass and the 20 minutes ball-milled glass. This shift is too large to be
47 ascribed to an artifact such as a sample displacement (max 0.1°). It can be noticed that this
48 **shifted peak** is located at the same angle as a diffraction line of the crystallized phase. It could
49 be due i) to a structural transformation of the initial glass into another polyamorph as already
50
51
52
53
54
55
56
57
58
59
60

1
2
3 observed in other chalcogenide glasses ^{16, 17}, ii) to the emergence of nanometric crystalline
4 domains, considering the low stability ($T_c - T_g$) of the glass ($\sim 30\text{K}$ ⁶) where T_c and T_g are the
5 crystallization and glass transition temperatures, respectively. Other evidences for this glass-
6 transformation will be further discussed below. PXRD also highlights crystallization
7 phenomenon which occurs during ball milling. After 45 min of ball-milling, some diffraction
8 lines appear at 29.58° and 44.89° (Fig.3). While they cannot be observed at $t_{\text{BM}} = 90$ min, they
9 appear again at $t_{\text{BM}} = 130$ min and become more intense for longer t_{BM} . Thus, the onset of
10 crystallization is ambiguous when considering only the XRD data. By combining the former
11 data with the DSC data (see Fig. 6), the beginning of crystallization can be better determined
12 to occur between $t_{\text{BM}} = 45$ min and $t_{\text{BM}} = 90$ min. These diffraction lines at 29.58° and 44.89°
13 are characteristic of one of the As_2Te_3 crystalline phases. Due to their very low intensity, it is
14 difficult to distinguish the $\alpha\text{-As}_2\text{Te}_3$ from the $\beta\text{-As}_2\text{Te}_3$ crystalline polymorphs based solely on
15 PXRD data. Nevertheless, the presence of the diffraction line near 45° is in favor of the
16 metastable $\beta\text{-As}_2\text{Te}_3$ form, which is likely to appear under out-of-equilibrium ball-milling
17 conditions in this specific glass composition ⁶.

18
19
20
21
22
23
24
25
26
27
28
29
30
31
32
33
34
35
36
37 The DSC curves, evidencing the temperatures of the glass transition, crystallization
38 and phase transformation, are plotted in Figure 4 for all the incremented t_{BM} . The DSC curve
39 of the reference $\text{Cu}_{15}\text{As}_{30}\text{Te}_{55}$ sample ($t_{\text{BM}} = 0$ min) shows an endothermic glass transition at
40 $T_g = 403$ K and a first crystallization peak at $T_{c1} = 440$ K. This crystallization peak is shifted
41 to higher temperature in comparison to our previous study ⁶. This enlightens the importance of
42 the particle size on the crystallization phenomenon which occurs in the present case at the
43 surface of the particles as already discussed in ¹⁸. Upon ball milling, T_g decreases to 399 K for
44 $t_{\text{BM}} = 90$ min (Table 2). For larger t_{BM} (samples are partially crystallized), the glass transition
45 is hidden by the first crystallization peak.

1
2
3
4
5 The first exothermic crystallization peak which extends from 440 K to 465 K in the
6 reference sample ($t_{BM} = 0$ min), is shifted to lower temperatures with t_{BM} (Table 2) in
7 accordance with the decrease of the particle size ¹⁹. A second weak peak is also observed
8 between 465 K and 480 K in the reference sample ($t_{BM} = 0$ min). Upon increasing the ball
9 milling durations, this peak separates into two components, which both shift towards lower
10 crystallization temperatures. In order to assess the crystalline composition, three 90 min
11 interrupted ball-milled $Cu_{15}As_{30}Te_{55}$ samples were heat-treated at a temperature higher than
12 the maximum of each three DSC peaks *i.e.* at 438, 459 and 478 K respectively, (black dots in
13 Figure 4) and their PXRD patterns were recorded. The results are displayed in Fig. 5. The
14 diffractogram recorded on the 438 K heat-treated sample can be indexed with metastable
15 β - As_2Te_3 as the major phase and $AsTe$ as a secondary phase. The first crystallization peak
16 observed in the DSC thermograms corresponds to the crystallization of these two phases, in
17 good agreement with a previous work ⁶. The second diffractogram at 459 K shows appearance
18 of diffraction lines corresponding to the $Cu_{1.4}Te$ rickardite phase. Thus, the second
19 crystallization peak can be ascribed to the crystallization of the rickardite phase. Finally, the
20 third diffractogram (Fig. 5) obtained after a heat-treatment at 478 K, shows diffraction peaks
21 related to the α - As_2Te_3 and $Cu_{1.4}Te$ phases indicating that the third DSC peak corresponds to
22 a β - to α - As_2Te_3 phase transition. For $t_{BM} = 180$ and 360 min, the intensity of the second and
23 third crystallization peaks hardly varies while the intensity of the first peak dramatically
24 decreases as seen in Fig. 4. This reduction in intensity could be related to the partial
25 crystallization of the glass particles into the β - As_2Te_3 crystalline phase upon ball-milling as
26 evidenced by the PXRD patterns shown in Fig. 3.

27
28
29
30
31
32
33
34
35
36
37
38
39
40
41
42
43
44
45
46
47
48
49
50
51
52 Based on the area A of the first crystallization peak, a glass transformation degree f
53 was defined and plotted in Fig. 6:
54
55

$$f = 100 \times \frac{A(t_{BM}=0) - A(t_{BM})}{A(t_{BM}=0)} \quad (1)$$

A sharp increase in the glass transformation degree for small t_{BM} is likely to arise from a transformation of the initial glass. As previously mentioned, this could be related to a nanostructuring of the grains. Nonetheless, the presence of a plateau following this sharp increase gives a highly non monotonous character to these variations. These are in favor of a glass-to-glass transformation (polyamorph), in agreement with both the shift of the main PXRD broad peak at $2\theta \sim 29^\circ$ and the change in the glass transition temperature T_g . For $t_{BM} > 45 - 90$ min, the increase in the glass transformation degree corresponds to the onset of the crystallization process during ball-milling and the presence of pre-existing crystallites, in good agreement with PXRD patterns (Fig. 3).

3.2 Glass-ceramics elaborated by SPS

In order to evaluate the effect of the ball-milling time on both the devitrification process and the thermoelectric properties, four series of $\text{Cu}_{15}\text{As}_{30}\text{Te}_{55}$ samples, ball-milled during various times (20, 45, 130 and 360 min) were sintered by SPS and compared to the reference sample sintered from hand-ground glass powder ($t_{BM} = 0$ min). During the sintering, a competition may occur between the glass particle sintering through a viscous flow mechanism and the crystallization phenomenon that occurs at the same time since the thermal stability of this specific glass composition is rather low ($\Delta T = 38\text{K}$), as discussed previously⁶.

3.2.1. Microstructures

The microstructures of three characteristic sintered glass-ceramics obtained for $t_{BM} = 0, 20$ and 360 min are presented in Fig. 7. The grain size after the SPS process on hand-ground samples is around $10 \mu\text{m}$, whereas the grain size after the SPS process on the 20 minutes ball-milled sample is around 200 nm . The same grain size is observed for $t_{BM} = 360$

1
2
3 minutes. Ball-milled samples display the same microstructure and thus, cannot be
4
5 differentiated by this feature. EDX maps reveal some differences in the chemical
6
7 homogeneity of the non-ball-milled and ball-milled samples ($t_{BM} = 0$ and 20 minutes). While
8
9 Te and As elements are well distributed within the matrix for both samples, Cu element is
10
11 found as aggregates with micrometric size in the sample $t_{BM} = 0$ min (Fig. 7g). These
12
13 aggregates, corresponding mostly to the crystallization of the $Cu_{1.4}Te$ rickardite phase, are
14
15 more homogeneously distributed in the sample $t_{BM} = 20$ minutes for comparison (Fig. 7h). As
16
17 will be further discussed, the fraction of crystalline phases is the critical parameter that best
18
19 characterizes the samples.
20
21
22
23

24 3.2.2. *Volume fractions of crystals and "glass rate"*

25
26 Figure 8 shows a typical PXRD pattern of a sintered glass-ceramic sample ($t_{BM} =$
27
28 130 min, SPS dwell time = 0 min, 80MPa, 423K). A remaining quantity of glass is
29
30 accompanied by four crystalline phases: α - As_2Te_3 ²⁰, β - As_2Te_3 ²⁰, $AsTe$ ^{21, 22} and $Cu_{1.4}Te$ ²³.
31
32 Rietveld refinements were performed to evaluate the relative crystalline phase fractions,
33
34 which are presented in Table 1. A **glass rate** was defined by integrating the area under the
35
36 main XRD peak around $2\theta = 29.58^\circ$, normalized to the high angle background around $2\theta =$
37
38 59° .
39
40
41
42
43

44 Figure 9 presents the evolution of the crystalline fractions and the **glass rate** as a
45
46 function of the ball-milling time. It is obvious that these fractions do not vary monotonously.
47
48 The fraction of β - As_2Te_3 goes through a sharp maximum for short ball-milling times (until 20
49
50 and 45 min) and then slowly decreases for longer ball-milling times. On the contrary, the α -
51
52 As_2Te_3 crystalline phase initially displays the largest fraction in the non-ball-milled sample,
53
54
55
56
57
58
59
60

strongly decreases for short ball-milling times, and then slowly increases for longer durations. Meanwhile, the average crystalline fractions of $\text{Cu}_{1.4}\text{Te}$ and AsTe phases remain under 20 wt% and their variance is relatively large.

These evolutions of the crystalline phase fractions are in good agreement with the evolution of the glass transformation degree plotted in Fig.6. For short t_{BM} (< 45 min), the large fraction of $\beta\text{-As}_2\text{Te}_3$ phase is correlated to the first glass-to-glass transformation. Indeed, it appears that this glass-to-glass transformation yields a glass reorganization which favors the germination of the metastable $\beta\text{-As}_2\text{Te}_3$ phase at the sintering stage. On the other hand, for longer t_{BM} , the crystallization, which occurs during ball-milling, favors larger fractions of the $\alpha\text{-As}_2\text{Te}_3$ phase at the SPS stage. The larger amount of energy provided by long t_{BM} finally favors the crystallization of the most thermodynamically stable phase, $\alpha\text{-As}_2\text{Te}_3$. Figure 9 gathers all the densified samples regardless of the sintering pressure (50 or 80 MPa). Since no distinction can be made between the samples, this parameter has no or a negligible influence on the phase fractions. Regarding the glass rate in the glass-ceramics, no trend can be noticed in the plot of the normalized glass rate versus t_{BM} .

3.2.3. Thermal and electrical transport properties

Figure 10 shows the Seebeck coefficient, the electrical resistivity, the thermal conductivity, and ZT of the SPS glass-ceramics as a function of t_{BM} . All the data shown here were measured at 400 K and are also summarized in Table 1. On the one hand, the evolution of the Seebeck coefficient with the ball-milling time mimics the evolution of the $\beta\text{-As}_2\text{Te}_3$ crystalline fraction up to $t_{\text{BM}} = 45$ min. For longer t_{BM} , the Seebeck coefficient weakly varies despite the decrease of the $\beta\text{-As}_2\text{Te}_3$ fraction. This arises from the increase of the $\alpha\text{-As}_2\text{Te}_3$ phase fraction, which also presents good thermoelectric properties²⁴. Although the values of the thermal conductivity present a high variability in the non-ball-milled sintered samples,

1
2
3 similarly to the Seebeck coefficient, they are correlated to t_{BM} and to the crystalline phase
4 fractions, *e.g.* they decrease in the ball-milled samples. For long ball-milling times, the values
5 weakly varies since the α -As₂Te₃ and β -As₂Te₃ phases display similar values of thermal
6 conductivities (1.0 W m⁻¹ K⁻¹ and 1.4 W m⁻¹ K⁻¹, respectively)^{7,24}. An effect of the numerous
7 interfaces created by the fine microstructure (~ 200 nm) on the phonon transport cannot as
8 well be excluded to explain this trend. Note that (i) the variability for $t_{BM} = 0$ min can
9 probably be related to the extremely variable remaining glass fraction for these samples (Fig.
10 9); (ii) the fact that the thermal conductivity reaches 1.8 W.m⁻¹.K⁻¹, while the thermal
11 conductivity of the Cu₁₅As₃₀Te₅₅ parent glass is about 0.22 W.m⁻¹.K⁻¹, or that of the α or β -
12 As₂Te₃ crystalline phase does not exceed 1.0 W m⁻¹ K⁻¹²⁴ and 1.4 W m⁻¹ K⁻¹, respectively⁷
13 could be explained by the presence of additional metallic phases, namely the Cu_{1.4}Te
14 rickardite²⁵ and AsTe²².

15
16
17
18
19
20
21
22
23
24
25
26
27
28
29
30
31
32
33
34
35
36
37
38
39
40
41
42
43
44
45
46
47
48
49
50
51
52
53
54
55
56
57
58
59
60
On the other hand, the resistivity values are subjected to a larger sample-to-sample
variability, which probably masks the evolution of this property. The values for all the
samples vary in an interval (± 0.60 m Ω cm) around the average value of 1.5 m Ω cm but
weakly influence the ZT values. This variability stems from: (i) the differences in crystalline
phases fractions; (ii) the likely different carrier concentrations of the As₂Te₃ phases, known
for severely impacting their electrical properties, especially in the case of α -As₂Te₃²⁶.

The figure of merit ZT follows the variations in the Seebeck coefficient: it goes
through a maximum for short t_{BM} , and weakly changes for longer t_{BM} . Again, this evolution
mimics the evolution of the β -As₂Te₃ phase fraction, which improves the thermoelectric
properties of the glass-ceramics. This result is in full agreement with our previous work on the
partial crystallization of the Cu₁₅As₃₀Te₅₅ glass composition which enabled an increase in the
 ZT values from 0.08 to 0.14 at 365K by crystallizing the metastable β -As₂Te₃ phase⁶. Indeed,
this phase was shown to display good thermoelectric properties at 400 K with $ZT = 0.4$ ⁷. In

1
2
3 the present work, the effect of short ball-milling time leads to an increase in the ZT_{\max} value,
4
5 from 0.15 for the best non-ball-milled sample to 0.3 at 400K for $t_{\text{BM}} = 20$ min.
6
7

8 **4. Conclusions**

10 In this study, the effect of ball-milling and crystallization from the $\text{Cu}_{15}\text{As}_{30}\text{Te}_{55}$
11 parent glass on the thermoelectric properties of the corresponding glass-ceramic materials are
12 presented. The partial crystallization of glass remains an interesting and original way to
13 stabilize new crystalline phases. Thanks to ball-milling, the grain size is reduced to less than
14 100 nm. PXRD and DSC measurements indicate that the first stages ($t_{\text{BM}} < 45$ min) induce a
15 glass-to-glass transformation followed by the crystallization of the $\beta\text{-As}_2\text{Te}_3$ phase which
16 occurs after $t_{\text{BM}} = 130$ min for interrupted ball-milling. Upon sintering, the grain size
17 increases up to 200 nm in every ball-milled sample. Four crystalline phases, namely $\alpha\text{-As}_2\text{Te}_3$,
18 $\beta\text{-As}_2\text{Te}_3$, AsTe and $\text{Cu}_{1.4}\text{Te}$, were evidenced in the different samples in various proportions.
19 The fraction of the metastable $\beta\text{-As}_2\text{Te}_3$ phase is maximum for short t_{BM} (20 - 45 min), *i.e.* for
20 samples which underwent the glass-to-glass transformation (in comparison to non-ball-milled
21 samples). These samples exhibit the largest thermoelectric figure of merit ZT up to 0.3 at
22 400K, a value nearly doubled when compared to the non-ball-milled glass-ceramics.
23
24
25
26
27
28
29
30
31
32
33
34
35
36
37
38
39
40

41 **Acknowledgements**

42 The authors would like to thank financial support from the French National Agency (ANR) in
43 the frame of its program "PROGELEC" (Verre Thermo-Générateur "VTG"). The authors
44 warmly thank Olivier Rouleau for thermoelectric measurements.
45
46
47
48
49
50
51
52
53
54
55
56
57
58
59
60

References

1. Parthasarathy G, Bandyopadhyay AK, Asokan S, Gopal ESR. Effect of pressure on the electrical resistivity of bulk $\text{Ge}_{20}\text{Te}_{80}$ glass. *Solid State Commun.* 1984; 51(4):195-7.
2. Dariush S. Seebeck coefficient of tellurite–vanadate glasses containing molybdenum. *J Phys D: Appl Phys.* 2008; 41(10):105102.
3. Pereira Goncalves A, Branco Lopes E, Rouleau O, Godart C. Conducting glasses as new potential thermoelectric materials: the Cu-Ge-Te case. *J Mater Chem.* 2010; 20(8):1516-21.
4. Gonçalves AP, Delaizir G, Lopes EB, Ferreira LM, Rouleau O, Godart C. Chalcogenide Glasses as Prospective Thermoelectric Materials. *J Electron Mater.* 2011; 40(5):1015-7.
5. Gonçalves AP, Lopes EB, Delaizir G, Vaney JB, Lenoir B, Piarristeguy A, et al. Semiconducting glasses: A new class of thermoelectric materials? *J Solid State Chem.* 2012; 193:26-30.
6. Vaney JB, Delaizir G, Alleno E, Rouleau O, Piarristeguy A, Monnier J, et al. A comprehensive study of the crystallization of Cu-As-Te glasses: microstructure and thermoelectric properties. *Journal of Materials Chemistry A.* 2013; 1(28):8190-200.
7. Vaney J-B, Carreaud J, Delaizir G, Pradel A, Piarristeguy A, Morin C, et al. High-Temperature Thermoelectric Properties of Sn-Doped $\beta\text{-As}_2\text{Te}_3$. *Advanced Electronic Materials.* 2015; 1:1400008.
8. Vaney JB, Piarristeguy A, Ohorodniichuck V, Ferry O, Pradel A, Alleno E, et al. Effective medium theory based modeling of the thermoelectric properties of composites: comparison between predictions and experiments in the glass-crystal composite system $\text{Si}_{10}\text{As}_{15}\text{Te}_{75}\text{-Bi}_{0.4}\text{Sb}_{1.6}\text{Te}_3$. *Journal of Materials Chemistry C.* 2015; 3(42):11090-8.

- 1
2
3 9. Landauer R. The Electrical Resistance of Binary Metallic Mixtures. *J Appl Phys.*
4
5 1952; 23(7):779-84.
6
- 7 10. Odelevski V. *Zh Tekh Fiz.* 1951; 21:678-85.
8
- 9 11. Webman I, Jortner J, Cohen MH. Thermoelectric power in inhomogeneous materials.
10
11 *Phys Rev B.* 1977; 16(6):2959-64.
12
- 13 12. McLachlan DS. An equation for the conductivity of binary mixtures with anisotropic
14
15 grain structures. *Journal of Physics C: Solid State Physics.* 1987; 20(7):865.
16
- 17 13. McLachlan DS, Blaszkiewicz M, Newnham RE. Electrical Resistivity of Composites.
18
19 *J Am Ceram Soc.* 1990; 73(8):2187-203.
20
- 21 14. Rouleau O, Alleno E. Measurement system of the Seebeck coefficient or of the
22
23 electrical resistivity at high temperature. *Rev Sci Instrum.* 2013; 84(10):105103.
24
- 25 15. Alleno E, Bérardan D, Byl C, Candolfi C, Daou R, Decourt R, et al. Invited Article: A
26
27 round robin test of the uncertainty on the measurement of the thermoelectric dimensionless
28
29 figure of merit of $\text{Co}_{0.97}\text{Ni}_{0.03}\text{Sb}_3$. *Rev Sci Instrum.* 2015; 86(1):011301.
30
31
- 32 16. Andrikopoulos KS, Christofilos D, Kourouklis GA, Yannopoulos SN. Pressure
33
34 dependence of the Boson peak in glassy As_2S_3 studied by Raman scattering. *J Non-Cryst*
35
36 *Solids.* 2006; 352(42-49):4594-600.
37
- 38 17. Calvez L, Lavanant E, Novikova A, Goncalves C, Bureau B, Nazabal V, et al. Te-As-
39
40 Se glass destabilization using high energy milling. *J Non-Cryst Solids.* 2018; 480:28-33.
41
- 42 18. Vaney J-B, Carreaud J, Piarristeguy A, Morin C, Delaizir G, Viennois R, et al.
43
44 Stabilization of Metastable Thermoelectric Crystalline Phases by Tuning the Glass
45
46 Composition in the Cu-As-Te System. *Inorg Chem.* 2018; 57:754-67.
47
- 48 19. Neuville DR, Cornier L, Caurant D, Montagne L. From glass to crystal: Nucleation,
49
50 growth and phase separation: from research to applications: EDP Sciences; 2017.
51
52
53
54
55
56

- 1
2
3 20. Morin C, Corallini S, Carreaud J, Vaney J-B, Delaizir G, Crivello J-C, et al.
4 Polymorphism in Thermoelectric As_2Te_3 . *Inorg Chem*. 2015; 54:9936 - 47.
5
6
7 21. Quinn RK. Compositional dependence of structural and thermal properties of arsenic-
8 tellurium amorphous alloys. *Mater Res Bull*. 1974; 9(6):803-13.
9
10
11 22. Johnson Jr RT, Quinn RK, Borders J. Electrical and structural properties of annealed
12 As- Te and As-Te-I semiconducting glasses: surface and bulk effects. *J Non-Cryst Solids*.
13 1974; 15(2):289-309.
14
15
16 23. Stevels ALN, Wiegers GA. Phase transitions in copper chalcogenides II. The tellurides
17 $\text{Cu}_{3-x}\text{Te}_2$ and CuTe . *Rec Trav Chim Pays-Bas*. 1971; 90(4):352-9.
18
19
20 24. Vaney J-B, Carreaud J, Delaizir G, Piarristeguy A, Pradel A, Alleno E, et al. High
21 Thermoelectric Performance in Sn-Substituted $\alpha\text{-As}_2\text{Te}_3$. *Journal of Materials Chemistry*
22 *C*. 2016; 4(12):2329-38.
23
24
25 25. Kobayashi K, Kawamoto S, Akimitsu J. Metallic binary copper chalcogenides with
26 orthorhombic layered structure. *MRS Online Proc Libr*. 2015; 1726(Emerging Non-Graphene
27 2D Atomic Layers and Van der Waals Solids):1-6.
28
29
30 26. Vaney JB, Carreaud J, Delaizir G, Morin C, Monnier J, Alleno E, et al. Thermoelectric
31 Properties of the $\alpha\text{-As}_2\text{Te}_3$ Crystalline Phase. *J Electron Mater*. 2016; 45(3):1447-52.
32
33
34
35
36
37
38
39
40
41
42
43
44
45
46
47
48
49
50
51
52
53
54
55
56
57
58
59
60

Figures captions

Figure 1: (a) SPS cycle of the reference sample (423 K, 80 MPa, dwell time = 30 min). Open squares are related to the temperature T inside the die and closed squares to load applied to the sample. (b) Corresponding shrinkage (mm) as a function of time during the same SPS cycle.

Figure 2: SEM micrographs of $\text{Cu}_{15}\text{As}_{30}\text{Te}_{55}$ powder obtained after different duration of ball milling $t_{\text{BM}} = 0$ (a), 2 (b), 20 (c) and 360 min (d) at low magnification and for $t_{\text{BM}} = 20$ (e) and 360 min (f, g) at high magnification.

Figure 3: PXRD of $\text{Cu}_{15}\text{As}_{30}\text{Te}_{55}$ powder after (a) continuously ball-milled at $t_{\text{BM}} = 20, 45$ and 130 min (Continuous BM), compared to the non-ball-milled glass ($t_{\text{BM}} = 0$ min) and (b) incrementally ball-milled at $t_{\text{BM}} = 20, 45, 90, 180$ and 360 min (Interrupted BM). The vertical dashed lines show the shift between non ball-milled and ball-milled glass and the black arrows show the diffraction line appearance. The baselines are different in panels (a) and (b) because of the different sample holders. The hump observed at 38° for continuous ball-milled samples is an artifact of the sample holder.

Figure 4: DSC thermograms of the $\text{Cu}_{15}\text{As}_{30}\text{Te}_{55}$ powders for various ball milling times. Black dots correspond to different annealing temperatures (438, 459 and 478 K, see text).

Figure 5: PXRD of 90 min ball-milled $\text{Cu}_{15}\text{As}_{30}\text{Te}_{55}$ powder after heat-treatments at 438, 459 and 478 K (■ - $\beta\text{-As}_2\text{Te}_3$, * - AsTe, ▲ - $\text{Cu}_{1.4}\text{Te}$ (rickardite) phases and □ - $\alpha\text{-As}_2\text{Te}_3$).

Figure 6: Glass transformation degree f as a function of ball-milling time t_{BM} . Squares are related to the incrementally ball-milled batch. Triangles are related to three other batches ball-milled without interruption during $t_{\text{BM}} = 20, 45, 130$ min. The continuous line is a spline through the entire dataset.

Figure 7: SEM micrographs of SPS glass-ceramics at two magnifications ($\times 1k$ and $\times 10k$) ; a & b: the hand-ground reference ($t_{\text{BM}} = 0$ min) ; c & d : $t_{\text{BM}} = 20$ min ball-milled sample; e & f : $t_{\text{BM}} = 360$ min. SPS was performed at 423 K with 10 min dwell time, under a pressure of 50 MPa (reference and $t_{\text{BM}} = 360$ min) or 80 MPa ($t_{\text{BM}} = 20$ min). Elemental EDX maps of these last two samples: $t_{\text{BM}} = 0$ min (g) and $t_{\text{BM}} = 20$ min (h).

Figure 8: PXRD patterns of a SPS sample ($t_{\text{BM}} = 130$ min, dwell 0 min, 80MPa, 423 K) between 10 and 60° . The main characteristic diffraction lines of $\text{Cu}_{1.4}\text{Te}$, AsTe, $\alpha\text{-As}_2\text{Te}_3$ and $\beta\text{-As}_2\text{Te}_3$ and the contribution of glass to the background (gray zone) are shown.

Figure 9: a-c. Crystallized phase fractions extracted from Rietveld refinements and d. normalized glass rate extracted from the SPSed glass-ceramics patterns, plotted as a function of t_{BM} . The solid lines represents the mean of phase fractions for each t_{BM} . The grey area is plotted to recall that the corresponding samples were partially crystallized after ball-milling.

Figure 10: a. Seebeck coefficient, b. electrical resistivity, c. thermal conductivity, and d. figure of merit ZT at 400 K for the SPS (See Table 1 for the SPS conditions) glass-ceramics as a function of t_{BM} . The solid lines represent the mean of transport properties for each t_{BM} . The grey area is plotted to recall that the corresponding samples were partially crystallized after ball-milling.

Table captions

Table 1: Ball-milling times t_{BM} , experimental SPS conditions ($T = 423K$, dwell time, pressure and maximal temperature in SPS T_{max}), density, crystallized phase fractions (extracted from Rietveld refinement), normalized glass rate, and thermoelectric properties measured at 400K.

Table 2: Glass transition T_g and first crystallization T_c temperatures of the $Cu_{15}As_{30}Te_{55}$ sample as a function of the ball milling time t_{BM} .

For Peer Review

Table 1: Ball-milling times t_{BM} , experimental SPS conditions ($T = 423K$, dwell time, pressure and maximal temperature in SPS T_{max}), density, crystallized phase fractions (extracted from Rietveld refinement), normalized glass rate, and thermoelectric properties measured at 400K.

t_{BM} (min)	SPS Conditions:	T_{max} (K)	Density	Crystallized phase fractions from Rietveld refinements (%mass)				Glass rate normalized toward background*	Seebeck coefficient ($\mu V.K^{-1}$)	Resistivity ($m\Omega.cm$)	Thermal conductivity ($W.m^{-1}.K^{-1}$)	ZT
				α - As ₂ Te ₃	β -As ₂ Te ₃	Cu _{1.4} Te	AsTe					
				0	0 min / 80 MPa	425.4	6.17					
0	10 min / 80 MPa	427.4	6.29	69	0	22	9	0.14	76	1.7	1.8	0.08
0	20 min / 80 MPa	428.3	6.32	69	12	15	5	0.13	77	1.2	1.5	0.13
0	30 min / 80 MPa	426.9	6.24	55	10	18	16	0.19	76	1.4	1.6	0.10
0	0 min / 50 MPa	427.9	6.31	64	0	19	17	0.08	81	-	-	-
0	10 min / 50 MPa	425.4	6.22	34	64	2	0	0.28	77	1.3	1.2	0.15
0	20 min / 50 MPa	430.3	6.31	64	13	20	4	0.11	76	1.3	1.6	0.11
20	0 min / 80 MPa	425.9	6.28	0	95	5	0	0.18	94	1.4	0.9	0.29
20	10 min / 80 MPa	428.4	6.34	54	10	18	18	0.09	101	2.3	-	-
20	20 min / 80 MPa	426.9	6.34	10	56	16	18	0.16	87	-	-	-
45	0min/80MPa	423.0	6.29	0	90	8	2	0.25	91	1.4	-	-
45	10min/80MPa	423.5	6.33	0	91	9	0	0.25	89	1.4	1.0	0.24
45	20min/80MPa	423.5	6.26	0	88	10	2	0.28	93	1.5	0.9	0.26
130	0 min / 50 MPa	426.9	6.34	38	44	5	13	0.21	91	1.4	1.0	0.22
130	10 min / 50 MPa	426.9	6.29	25	59	4	12	0.20	86	1.6	1.0	0.19
130	20 min / 50 MPa	425.9	6.25	24	43	15	18	0.22	86	1.7	1.0	0.17
360	0 min / 50 MPa	423.0	6.24	43	16	22	19	0.33	91	1.3	1.1	0.23
360	10 min / 50 MPa	423.0	6.27	45	14	22	19	0.34	92	-	-	-
360	20 min / 50 MPa	425.0	6.30	0	62	38	0	0.20	91	1.2	1.2	0.24

*The values have been normalized to the 100% glassy compound,

Table 2: Glass transition T_g and first crystallization T_c temperatures of the $\text{Cu}_{15}\text{As}_{30}\text{Te}_{55}$ sample as a function of the ball milling time t_{BM} .

	Incremental ball-milling (= interrupted BM)								Continuous BM		
t_{BM} (min)	0	2	8	20	45	90	180	360	20	45	130
T_g (K)	402.9(5)	402.2(5)	401.0(5)	400.2(5)	400.3(5)	398.7(5)			397.0(5)	394.1(5)	
T_c (K)	440(1)	420(1)	414(1)	412(1)	411(1)	411(1)	404(1)	403(1)	411(1)	410(1)	407(1)

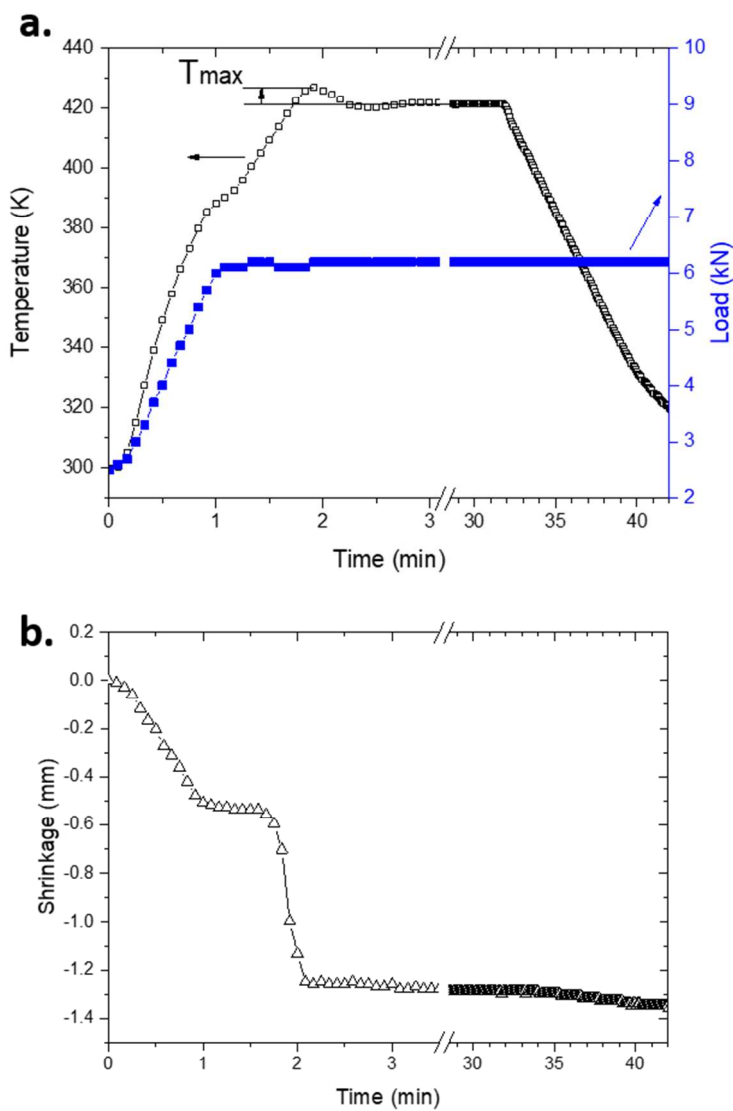


Figure 1: (a) SPS cycle of the reference sample (423 K, 80 MPa, dwell time = 30 min). Open squares are related to the temperature T inside the die and closed squares to load applied to the sample. (b) Corresponding shrinkage (mm) as a function of time during the same SPS cycle.

115x169mm (150 x 150 DPI)

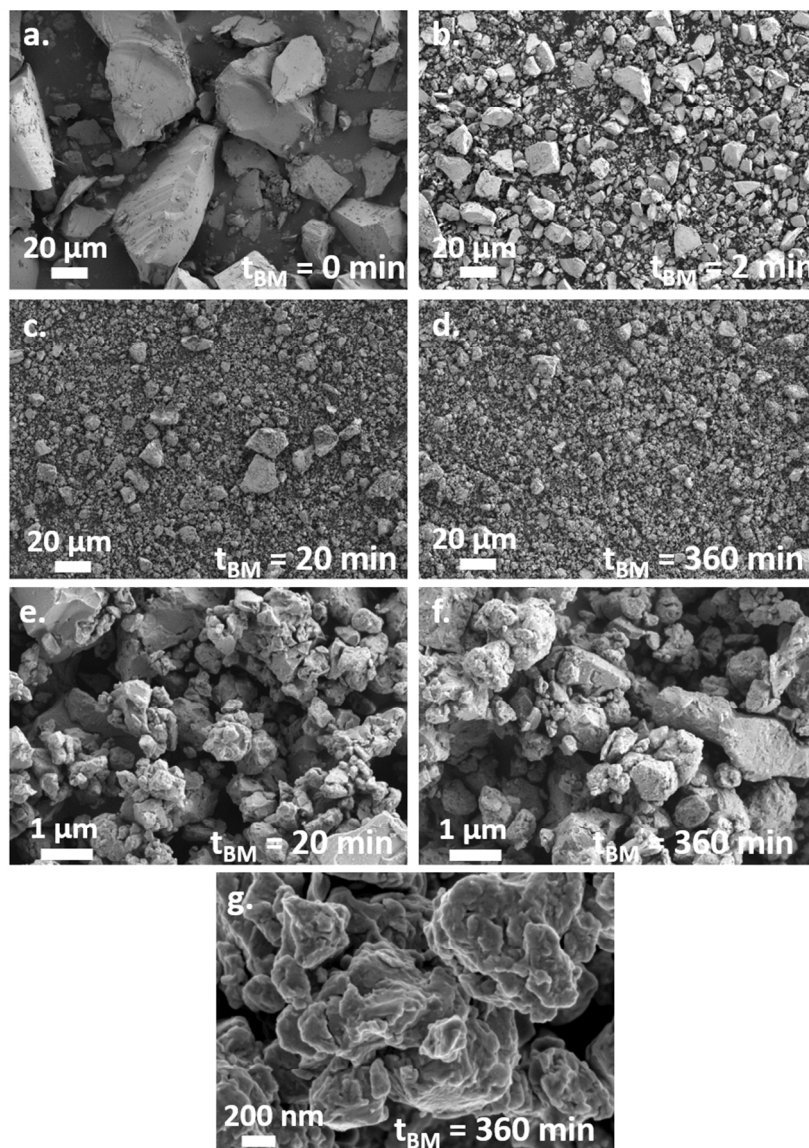


Figure 2: SEM micrographs of Cu₁₅As₃₀Te₅₅ powder obtained after different duration of ball milling t_{BM} = 0 (a), 2 (b), 20 (c) and 360 min (d) at low magnification and for t_{BM} = 20 (e) and 360 min (f, g) at high magnification.

174x235mm (150 x 150 DPI)

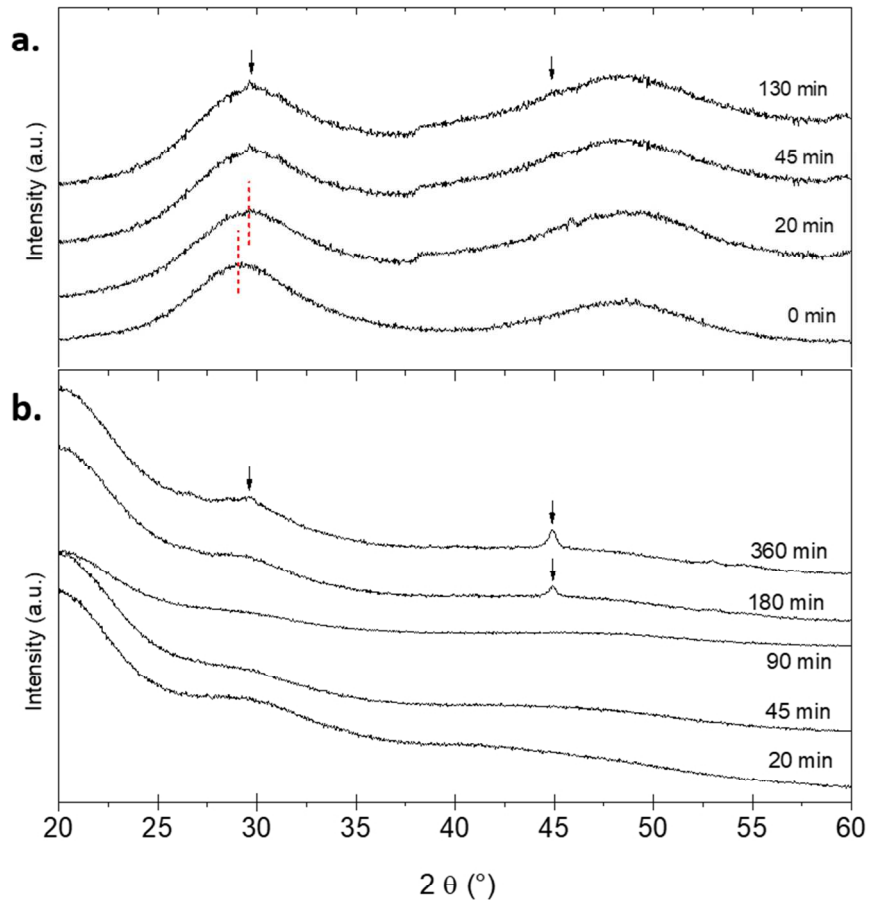


Figure 3: PXRD of Cu₁₅As₃₀Te₅₅ powder after (a) continuously ball-milled at tBM = 20, 45 and 130 min (Continuous BM), compared to the non-ball-milled glass (tBM = 0min) and (b) incrementally ball-milled at tBM = 20, 45, 90, 180 and 360 min (Interrupted BM). The vertical dashed lines show the shift between non ball-milled and ball-milled glass and the black arrows show the diffraction line appearance. The baselines are different in panels (a) and (b) because of the different sample holders. The hump observed at 38° for continuous ball-milled samples is an artifact of the sample holder.

160x167mm (150 x 150 DPI)

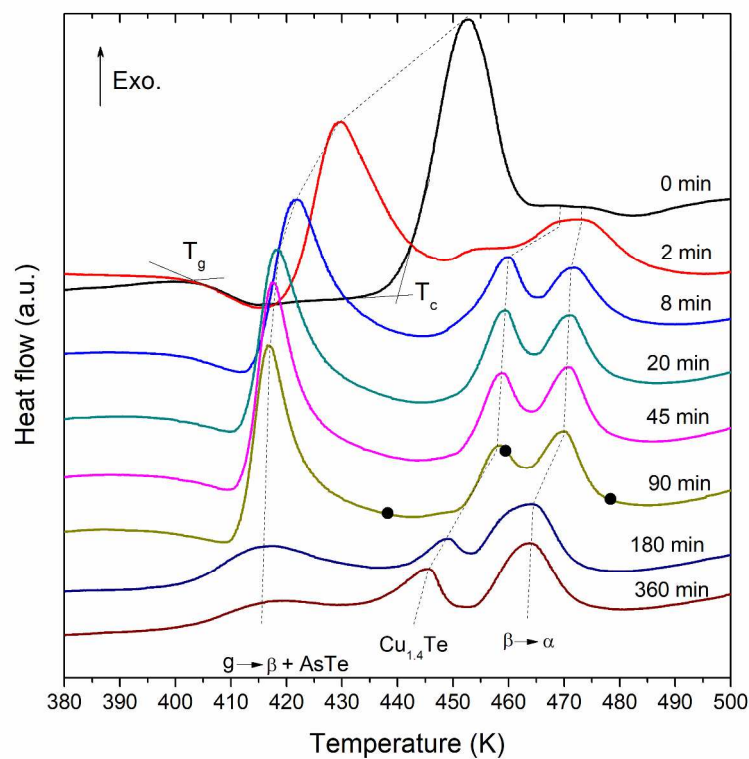


Figure 4: DSC thermograms of the $\text{Cu}_{15}\text{As}_{30}\text{Te}_{55}$ powders for various ball milling times. Black dots correspond to different annealing temperatures (438, 459 and 478 K, see text).

299x249mm (300 x 300 DPI)

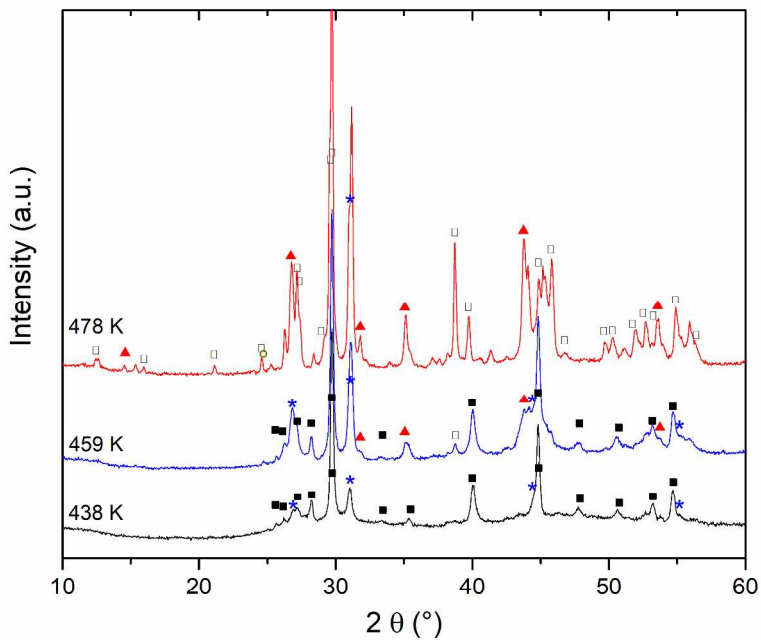


Figure 5: PXRD of 90 min ball-milled $\text{Cu}_{15}\text{As}_{30}\text{Te}_{55}$ powder after heat-treatments at 438, 459 and 478 K (\square - $\beta\text{-As}_2\text{Te}_3$, \triangle - AsTe , \circ - $\text{Cu}_{1.4}\text{Te}$ (rickardite) phases and \bullet - $\alpha\text{-As}_2\text{Te}_3$)

272x208mm (300 x 300 DPI)

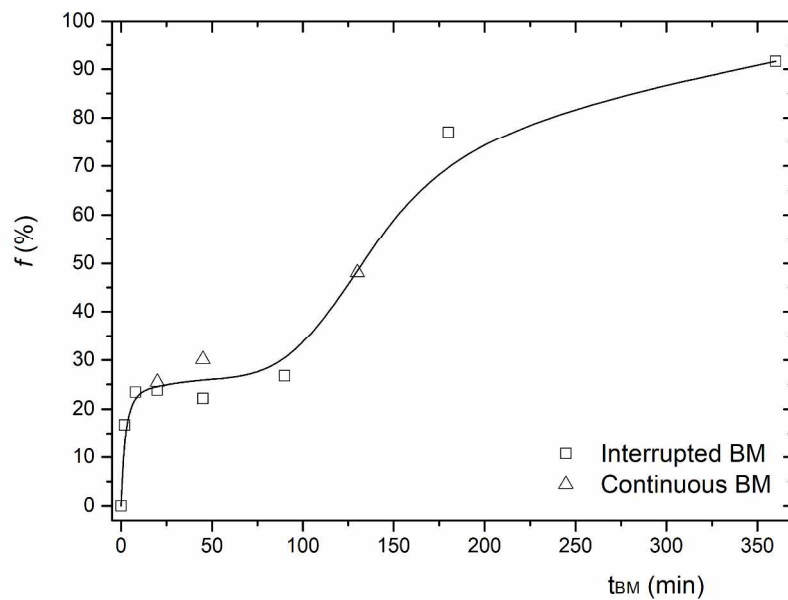


Figure 6: Glass transformation degree f as a function of ball-milling time t_{BM} . Squares are related to the incrementally ball-milled batch. Triangles are related to three other batches ball-milled without interruption during $t_{BM} = 20, 45, 130$ min. The continuous line is a spline through the entire dataset.

287x200mm (300 x 300 DPI)

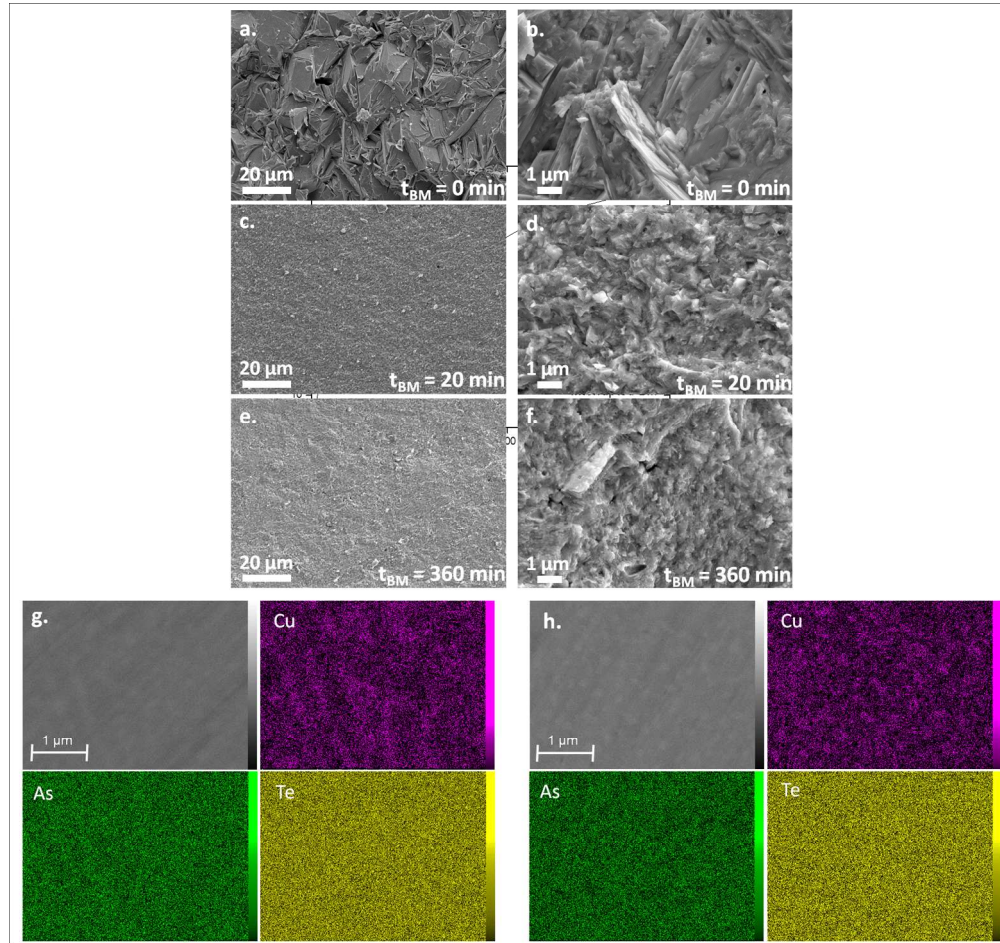


Figure 7: SEM micrographs of SPS glass-ceramics at two magnifications ($\times 1k$ and $\times 10k$); a & b: the hand-ground reference ($t_{BM} = 0$ min); c & d: $t_{BM} = 20$ min ball-milled sample; e & f: $t_{BM} = 360$ min. SPS was performed at 423 K with 10 min dwell time, under a pressure of 50 MPa (reference and $t_{BM} = 360$ min) or 80 MPa ($t_{BM} = 20$ min). Elemental EDX maps of these last two samples: $t_{BM} = 0$ min (g) and $t_{BM} = 20$ min (h).

307x290mm (150 x 150 DPI)

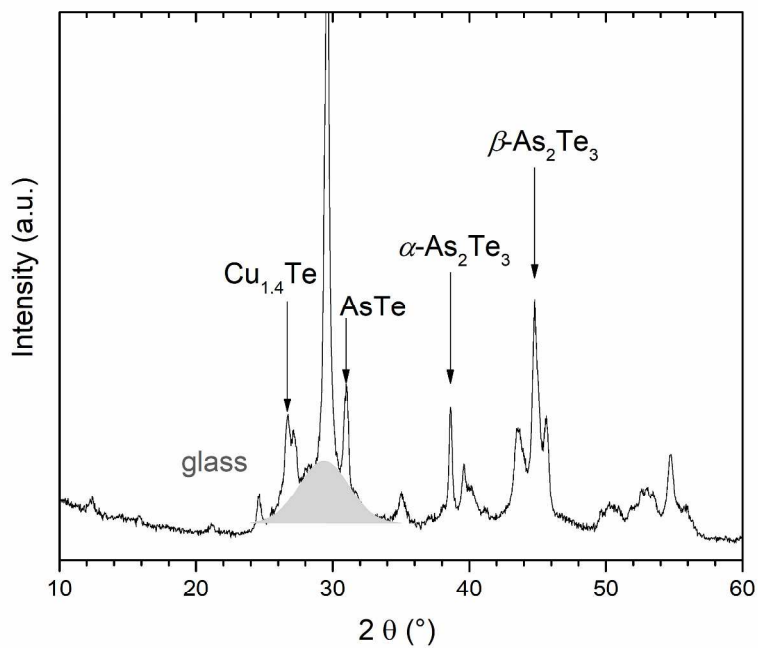


Figure 8: XRD patterns of a SPS sample (tBM =130 min, dwell 0 min, 80MPa, 423 K) between 10 and 60°. The main characteristic diffraction lines of Cu_{1.4}Te, AsTe, α-As₂Te₃ and β-As₂Te₃ and the contribution of glass to the background (gray zone) are shown.

272x208mm (300 x 300 DPI)

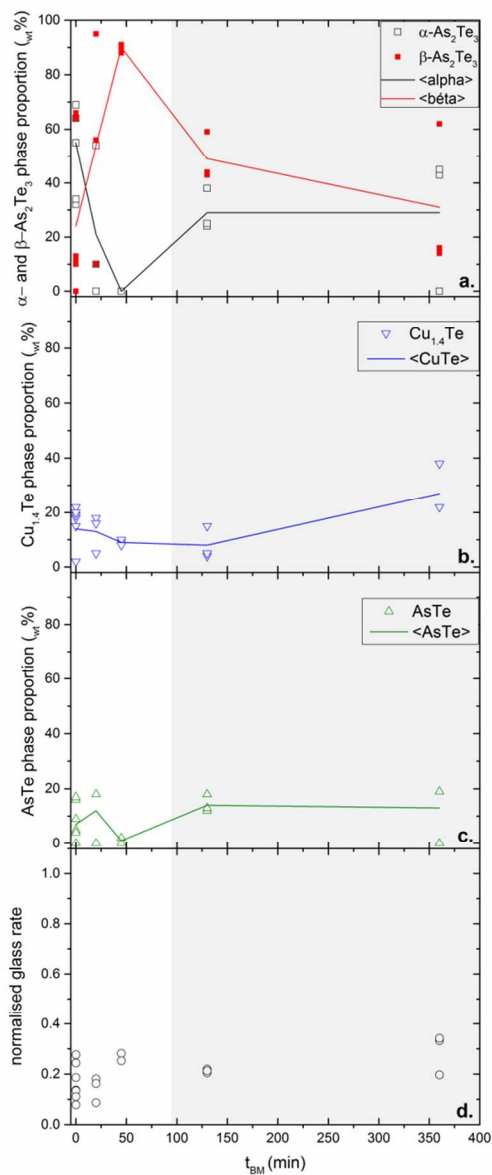


Figure 9: a-c. Crystallized phase fractions extracted from Rietveld refinements and d. normalized glass rate extracted from the SPSed glass-ceramics patterns, plotted as a function of t_{BM} . The solid lines represents the mean of phase fractions for each t_{BM} . The grey area is plotted to recall that the corresponding samples were partially crystallized after ball-milling.

108x237mm (150 x 150 DPI)

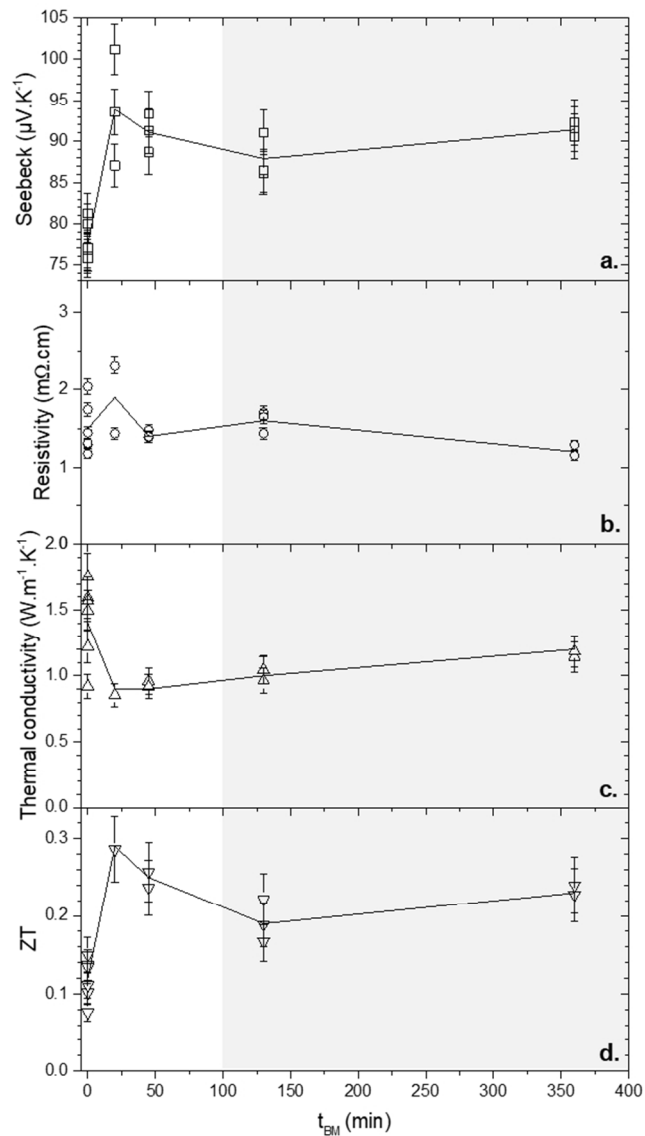
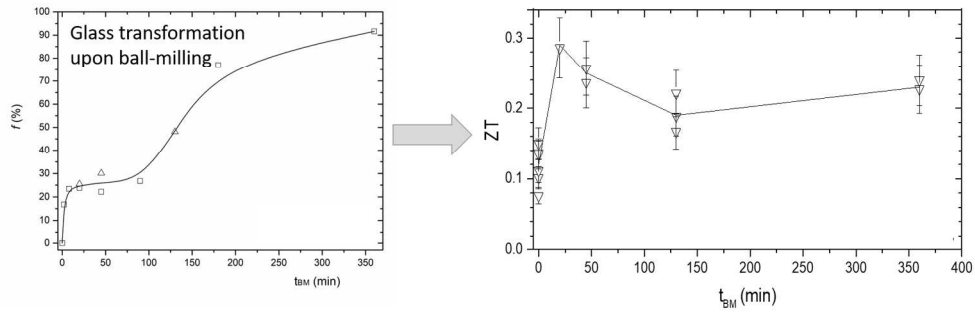


Figure 10: a. Seebeck coefficient, b. electrical resistivity, c. thermal conductivity, and d. figure of merit ZT at 400 K for the SPS (See Table 1 for the SPS conditions) glass-ceramics as a function of t_{BM} . The solid lines represent the mean of transport properties for each t_{BM} . The grey area is plotted to recall that the corresponding samples were partially crystallized after ball-milling.

119x194mm (150 x 150 DPI)

1
2
3
4
5
6
7
8
9
10
11
12
13
14
15
16
17
18
19
20
21
22
23
24
25
26
27
28
29
30
31
32
33
34
35
36
37
38
39
40
41
42
43
44
45
46
47
48
49
50
51
52
53
54
55
56
57
58
59
60



306x104mm (150 x 150 DPI)

Or Peer Review